

## EFFECTS OF FIVE DIFFERENT PARAMETERS ON BIODIESEL HCCI COMBUSTION IN FREE-PISTON ENGINE GENERATOR

by

**Chunhui LIU\*, Shaojie WU, and Shuo PANG**

College of Mechanical Engineering, Anhui Science and Technology University,  
Fengyang, China

Original scientific paper  
<https://doi.org/10.2298/TSCI2106197L>

*A coupled 3-D CFD and detailed chemical kinetics model of free-piston engine generator (FPEG) was adopted to investigate the effects of initial parameters on homogeneous charge compression ignition (HCCI) combustion and emission. Biodiesel with 115 species skeletal mechanism was selected as fuel. Five different parameters, namely the initial pressure, the initial temperature, the working frequency, the compression ratio and the fuel equivalence ratio, were selected to analyze their influences in the HCCI combustion simulation of FPEG. The simulation results showed that the change of the five parameters had visible impact on the heat release rate of HCCI combustion, which caused the in-cylinder temperature and pressure to change, and also caused the emission content of  $\text{NO}_x$  and SOOT to change obviously.*

Keywords: FPEG, skeletal mechanism, biodiesel, HCCI

### Introduction

As an efficient technology, HCCI, integrating the merit of the traditional Diesel engine and gasoline engine, has been attracting the attention of researchers due to its potential of low particulate and near zero-level  $\text{NO}_x$  emission [1-5]. However, the operation of HCCI in conventional internal combustion engine (ICE) has some challenges, such as the narrow work range and the uncontrollable auto-ignition moment. The control means of HCCI in the conventional ICE only include the fuel injection timing control and the exhaust gas recycling, which cannot fully utilize the advantages of HCCI.

The FPE [6], no crank connecting rod, has some potential merit, such as variable compression ratio, flexible piston movement speed, extensive fuel applicability, and so on [7], which can solve the problem of the HCCI combustion starting time and rate control.

From 1930's to 1960's, the air compressors had a rapid development on the basis of FPE introduced by Pescara in 1928 [8]. In recent decades, FPE are mainly applied for electric generator and hydraulic pumps [9]. For the electric generator, FPE with a linear electric generator, namely FPEG, is the most common form of implementation [10].

---

\*Corresponding author, e-mail: lch994211@163.com

Many FPEG prototype designs of different research institutions have been reported [8]. Several prototypes can bring about continuous output of energy conversion, and the power generation efficiency can achieve 34%. Biodiesel, a renewable alternative fuel, can be used in compression ignition engine and effectively reduce the harmful emissions. The obtainment of biodiesel has multiple sources, so wide application of biodiesel can reduce dependence on fossil fuels and can also protect environment by lowering emissions of harmful gas [11-16].

In this paper, a 3-D CFD model coupling a 115 species skeletal mechanism of biodiesel was established to investigate the HCCI combustion and emission performance of an opposed-piston two-stroke FPEG. Five different parameters, namely the initial pressure, the initial temperature, the working frequency, the compression ratio, and the fuel equivalence ratio, were selected to analyze their influences in the HCCI combustion simulation of FPEG.

### Coupled CFD and chemical kinetics model

The piston dynamics of FPEG is different from that of the traditional ICE, because FPEG has no crank connecting rod. The piston motion law of FPEG was commonly obtained by using the 0-D models including dynamic model, thermodynamic model, frictional model, and generator model. The structure and 0-D modeling of FPEG can see [17].

With the piston motion curve of FPEG (dual piston, two-stroke) calculated using the 0-D models and the key simulation parameters, the combustion chamber moving mesh model was created in fig. 1.

The detailed mechanism of biodiesel contains several thousand species, which makes it impossible to model the combustion process in the 3-D CFD model. So a 115 species skeletal mechanism [18] developed from the detailed mechanism and validated for compression ignition engine was applied in the 3-D CFD model. The extended Zel'dovich  $\text{NO}_x$  mechanism was used to calculate NO formation. The SOOT production was obtained through Hiroyasu-NSC model, and  $\text{C}_2\text{H}_2$  was used as the SOOT formation species.

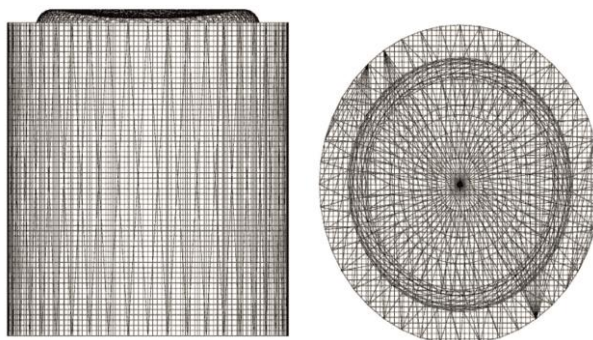


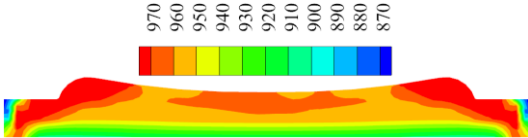
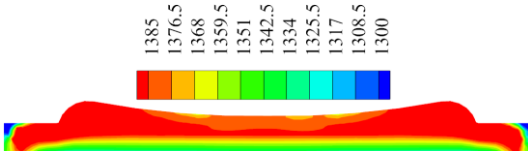
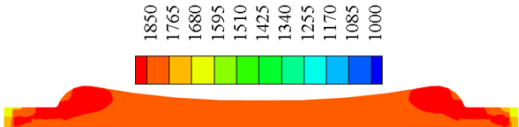
Figure 1. The combustion chamber moving mesh model

### Simulation

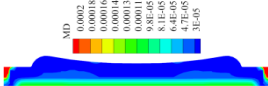
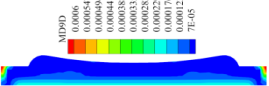
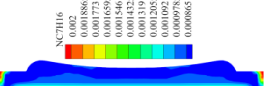
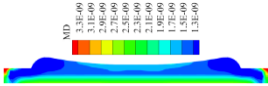
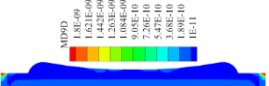
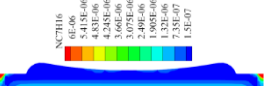
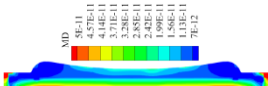
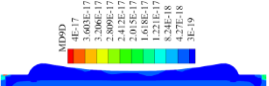
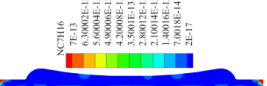
Three combustion stages, namely CA10, CA50, and CA90, were chosen to reveal the temperature and fuel concentration field distribution under the initial conditions of temperature 345 K, pressure 1.14 bar, fuel equivalent ratio 0.4, compression ratio 20.2, and working frequency 22.9. The CA10 was defined as the CA position for 10% of the cumulative heat release, while the CA50 and CA90 were defined in the same way. Table 1 demonstrated the distribution of calculated in-cylinder temperature field. The distribution of fuel concentration field was indicated in tab. 2.

At CA10, the temperature near piston bowl was the highest, where the fuel was most oxidized. At CA50, the temperature rose and the distribution of that began to be uniform, and the fuel was further consumed. At CA90, the temperature further increased and the distribution of that was almost uniform, and the almost all fuel was consumed.

**Table 1. The temperature field**

Combustion stage	Temperature field
CA10	 <p>Temperature scale for CA10: 970, 960, 950, 940, 930, 920, 910, 900, 890, 880, 870</p>
CA50	 <p>Temperature scale for CA50: 1385, 1376.5, 1368, 1359.5, 1351, 1342.5, 1334, 1325.5, 1317, 1308.5, 1300</p>
CA90	 <p>Temperature scale for CA90: 1850, 1765, 1680, 1595, 1510, 1425, 1340, 1255, 1170, 1085, 1000</p>

**Table 2. The fuel concentration field**

Combustion stage	Fuel concentration field		
CA10	 <p>MD</p> <p>0.0002 0.000183 0.000166 0.000151 0.000135 9.8E-05 9.8E-05 6.4E-05 4.7E-05 3E-05</p>	 <p>MD90</p> <p>0.0006 0.000547 0.000504 0.000461 0.000388 0.000335 0.000282 0.000229 0.000176 0.000123 7E-05</p>	 <p>NCTH16</p> <p>0.002 0.001865 0.001695 0.001546 0.001432 0.001325 0.001202 0.000975 0.000605</p>
CA50	 <p>MD</p> <p>3.3E-09 3.1E-09 2.9E-09 2.7E-09 2.5E-09 2.3E-09 2.1E-09 1.9E-09 1.7E-09 1.5E-09 1.3E-09</p>	 <p>MD90</p> <p>1.8E-09 1.62E-09 1.442E-09 1.264E-09 1.086E-09 9.08E-10 7.26E-10 5.47E-10 3.68E-10 1.89E-10 1E-11</p>	 <p>NCTH16</p> <p>6E-06 5.41E-06 4.82E-06 4.23E-06 3.64E-06 3.07E-06 2.5E-06 1.96E-06 1.32E-06 7.3E-07 1.5E-07</p>
CA90	 <p>MD</p> <p>5E-11 4.57E-11 4.14E-11 3.71E-11 3.28E-11 2.85E-11 2.42E-11 1.99E-11 1.56E-11 1.13E-11 7E-12</p>	 <p>MD90</p> <p>4E-17 3.603E-17 3.208E-17 2.808E-17 2.412E-17 2.015E-17 1.618E-17 1.221E-17 8.24E-18 4.27E-18 3E-19</p>	 <p>NCTH16</p> <p>7E-13 6.300E-13 5.600E-13 4.900E-13 4.200E-13 3.500E-13 2.800E-13 2.100E-13 1.400E-13 7.00E-14 2E-17</p>

### The effects of parameter change on combustion process

*Initial temperature*

Figure 2 showed the results of initial temperature change on combustion progress with working frequency  $f = 22.9$  Hz, fuel equivalence ratio  $\phi = 0.4$ , initial pressure  $P = 1.14$  bar, and compression ratio  $\varepsilon = 20.2$ . It was seen that when the initial temperature increased from 315 K to 375 K, the FPEG ignition time had  $5^\circ$  CA in advance, the peak value of in-cylinder temperature increased from 1922 K to 2111 K, maximum heat release rate increased from 104 J/ $^\circ$  to 141 J/ $^\circ$ , and maximum in-cylinder pressure decreased from 14.6 MPa to 13.4 MPa.

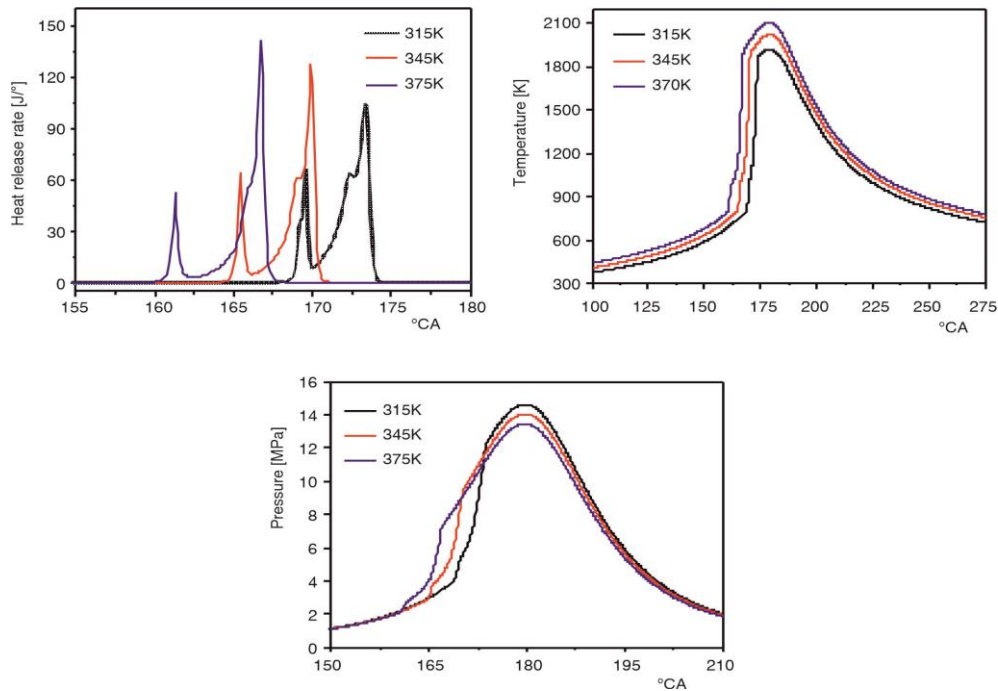


Figure 2. The results of initial temperature change

#### Initial pressure

Figure 3 indicated the results of different initial pressure on combustion progress with working frequency  $f = 22.9$  Hz, initial temperature  $T_0 = 345$  K, fuel equivalence ratio  $\phi = 0.4$ , and compression ratio  $\varepsilon = 20.2$ . It was noted that when the initial pressure increased from 1.14 bar to 1.46 bar, the FPEG combustion phase slightly advanced  $0.2^\circ$  CA, the maximum temperature and heat release rate slightly increased 13 K and 14 J/° separately, and maximum pressure obviously increased from 18 MPa to 14 MPa.

#### Fuel equivalence ratio

Figure 4 revealed the results of different fuel equivalence ratio on combustion progress with working frequency  $f = 22.9$  Hz, initial temperature  $T_0 = 345$  K, initial pressure  $P = 1.14$  bar, and compression ratio  $\varepsilon = 20.2$ . It was seen that when the fuel equivalence ratio increased from 0.3 to 0.45, the FPEG combustion phase delayed  $1.2^\circ$  CA, while the maximum heat release rate, pressure and temperature increased from 25 J/° to 252 J/°, 12.3 MPa to 14.9 MPa, 1790 K to 2130 K, separately.

#### Working frequency

Figure 5 demonstrated the results of different working frequency on combustion progress with fuel equivalence ratio  $\phi = 0.4$ , initial temperature  $T_0 = 345$  K, initial pressure  $P = 1.14$  bar, and compression ratio  $\varepsilon = 20.2$ . It was noted that when the working frequency increased from 19.6 Hz to 27.9 Hz, the FPEG combustion phase delayed  $1.3^\circ$  CA, while the maximum heat release rate, pressure and temperature remained basically unchanged (only changed 3 J/°, 0.01 MPa and 5 K, separately).

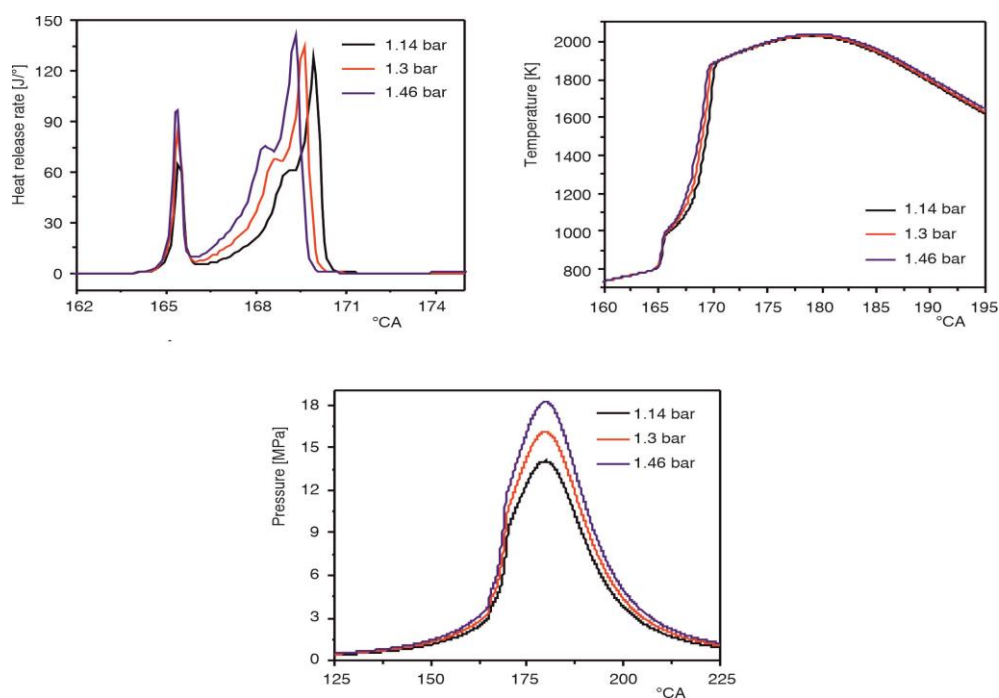


Figure 3. The results of initial pressure change

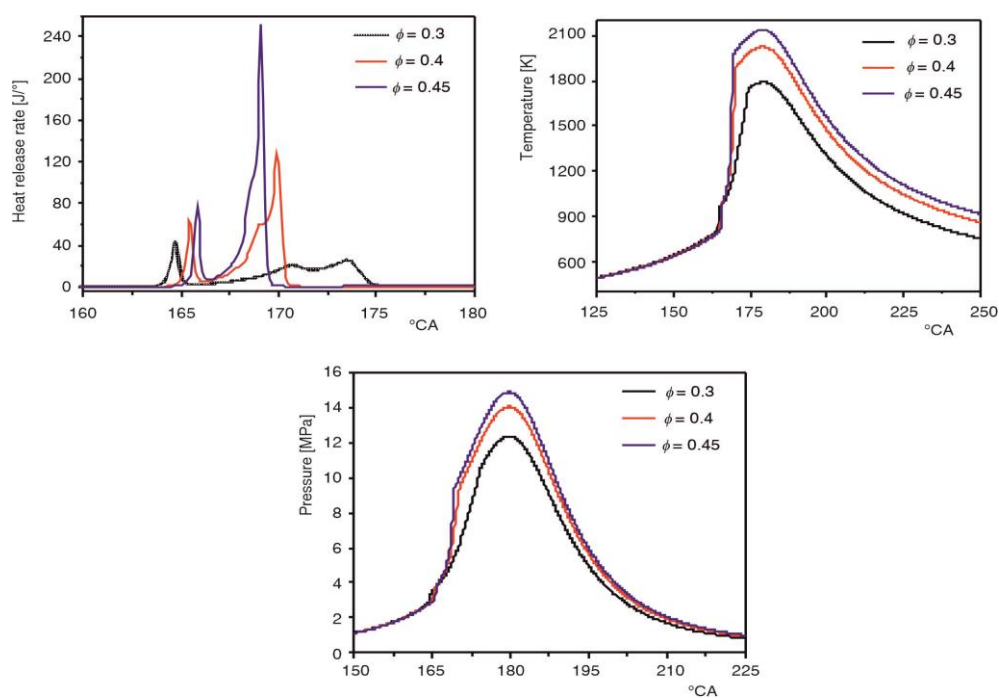


Figure 4. The results of fuel equivalence ratio change

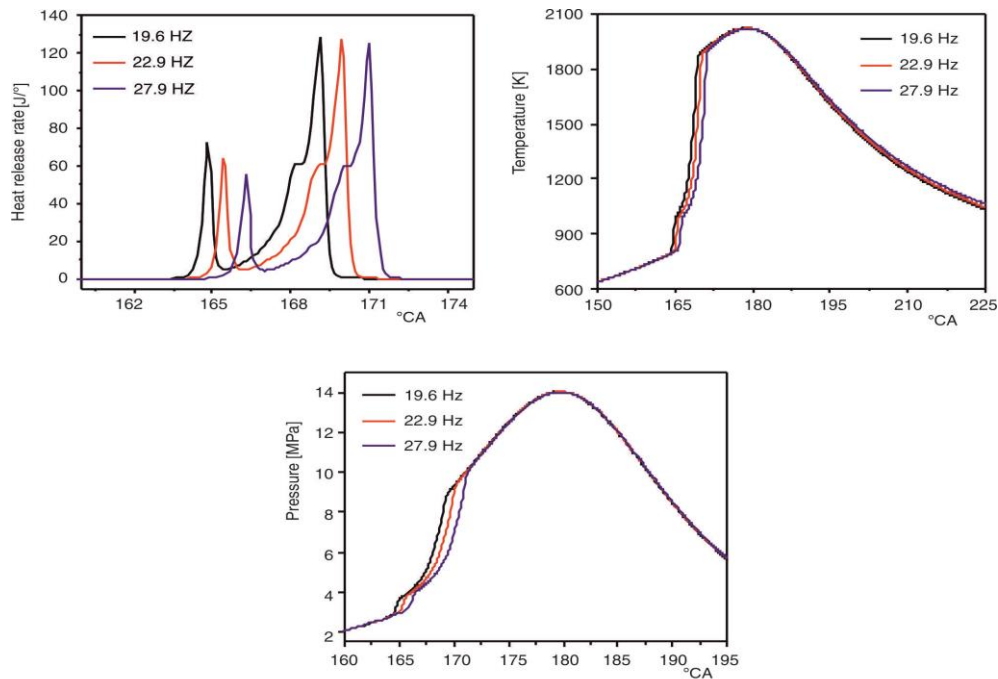


Figure 5. The results of working frequency change

### Compression ratio

Figure 6 showed the results of different compression ratio on combustion progress with working frequency  $f = 22.9$  Hz, initial temperature  $T_0 = 345$  K, initial pressure  $P = 1.14$  bar, and fuel equivalence ratio  $\phi = 0.4$ . It was seen that when the compression ratio increased from 15.9 to 20.2, the FPEG combustion phase advanced  $2.5^\circ$  CA, while the maximum heat release rate, pressure and temperature increased from  $108 \text{ J/}^\circ$  to  $127 \text{ J/}^\circ$ ,  $10.5 \text{ MPa}$  to  $14 \text{ MPa}$ ,  $1920 \text{ K}$  to  $2025 \text{ K}$ , separately.

### The effects of parameter change on emissions

#### Initial temperature

Figure 7 indicated the results of different initial temperature on emissions with working frequency  $f = 22.9$  Hz, initial pressure  $P = 1.14$  bar, fuel equivalence ratio  $\phi = 0.4$ , and compression ratio  $\varepsilon = 20.2$ . It was noted that as the initial temperature increased from  $315 \text{ K}$  to  $375 \text{ K}$ ,  $\text{NO}_x$  content significantly increased from  $0.18 \text{ g/Kg}$  fuel to  $7.1 \text{ g/Kg}$  fuel, while the consumption of UHC and the production of CO and SOOT were  $13^\circ$ ,  $9^\circ$ , and  $11^\circ$  CA in advance, separately.

#### Initial pressure

Figure 8 revealed the results of different initial pressure on emissions with working frequency  $f = 22.9$  Hz, initial temperature  $T_0 = 345 \text{ K}$ , fuel equivalence ratio  $\phi = 0.4$ , and compression ratio  $\varepsilon = 20.2$ . It was seen that as the initial pressure increased from  $1.14 \text{ bar}$  to  $1.46 \text{ bar}$ ,  $\text{NO}_x$  content increased from  $1.3 \text{ g/Kg}$  fuel to  $1.7 \text{ g/Kg}$  fuel, while the consumption of UHC and the production of CO and SOOT content were at almost the same CA, separately.

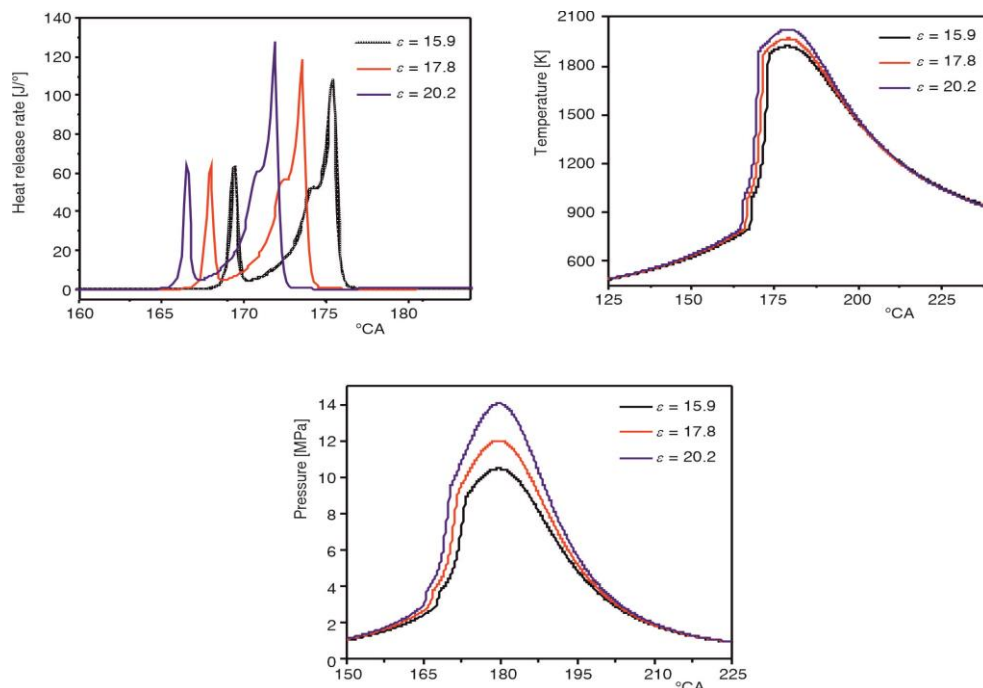


Figure 6. The results of compression ratio change

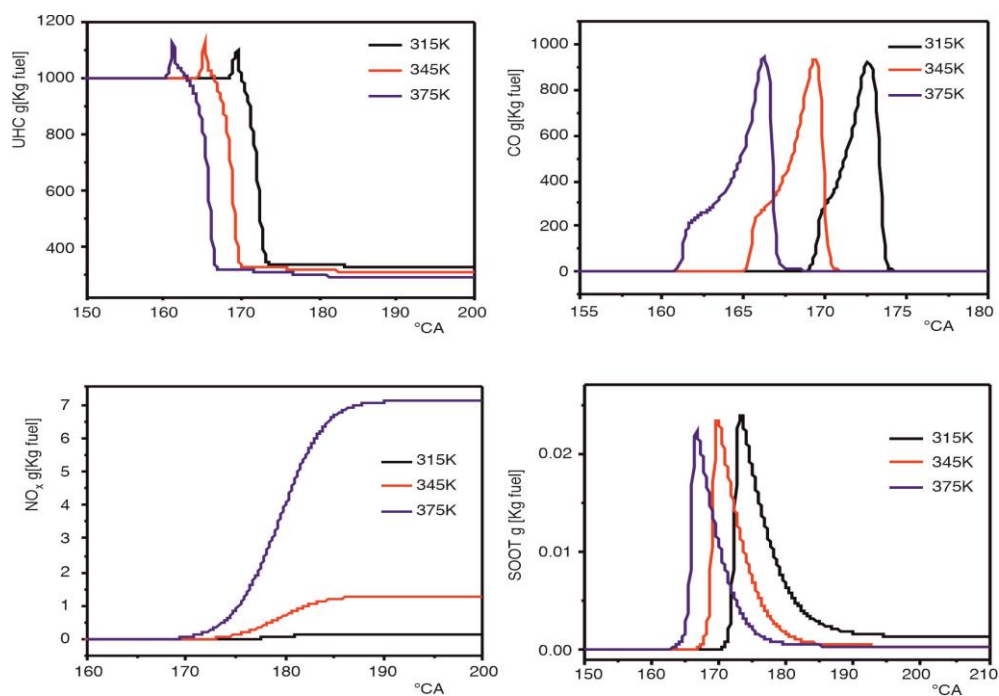


Figure 7. The results of initial temperature change



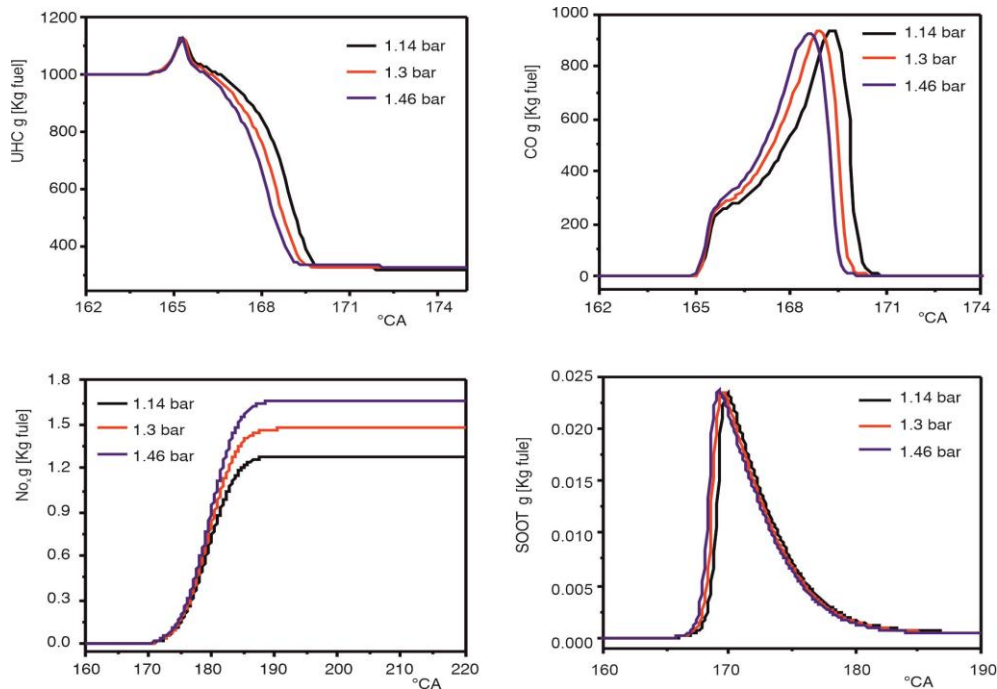


Figure 8. The results of initial pressure change

### Fuel equivalence ratio

Figure 9 demonstrated the results of different fuel equivalence ratio on emissions with working frequency  $f = 22.9$  Hz, initial temperature  $T_0 = 345$  K, initial pressure  $P = 1.14$  bar, and compression ratio  $\varepsilon = 20.2$ . It can be noted that because of the incomplete high thermal release heat release (fig. 5), when the fuel equivalent ratio equaled to 0.3, the NO<sub>x</sub> content was 0.02 g/Kg fuel. And as the fuel equivalent ratio increased from 0.3 to 0.45, the NO<sub>x</sub> content increased from 0.02 g/Kg fuel to 7.5 g/Kg fuel, while the consumption of UHC and the production of CO lagged 1.5° CA and 1.6° CA, and the production of SOOT advanced 1.2° CA.

### Working frequency

Figure 10 showed the results of different working frequency on emissions with fuel equivalence ratio  $\phi = 0.4$ , initial temperature  $T_0 = 345$  K, initial pressure  $P = 1.14$  bar, and compression ratio  $\varepsilon = 20.2$ . It was seen that as working frequency increased from 19.6 Hz to 27.9 Hz, NO<sub>x</sub> content decreased from 1.7 g/Kg fuel to 0.9 g/Kg fuel, while the consumption of UHC and the production of CO and SOOT lagged 1° CA, 1° CA, and 1.7° CA, separately.

### Compression ratio

Figure 11 demonstrated the results of different compression ratio on emissions with working frequency  $f = 22.9$  Hz, initial temperature  $T_0 = 345$  K, initial pressure  $P = 1.14$  bar, and fuel equivalence ratio  $\phi = 0.4$ . It was noted that as compression ratio increased from 15.9 to 20.2, NO<sub>x</sub> content increased from 0.17 g/Kg fuel to 1.29 g/Kg fuel, while the consumption of UHC and the production of CO and SOOT advanced 2.4° CA, 2.2° CA, and 2.6° CA, separately.



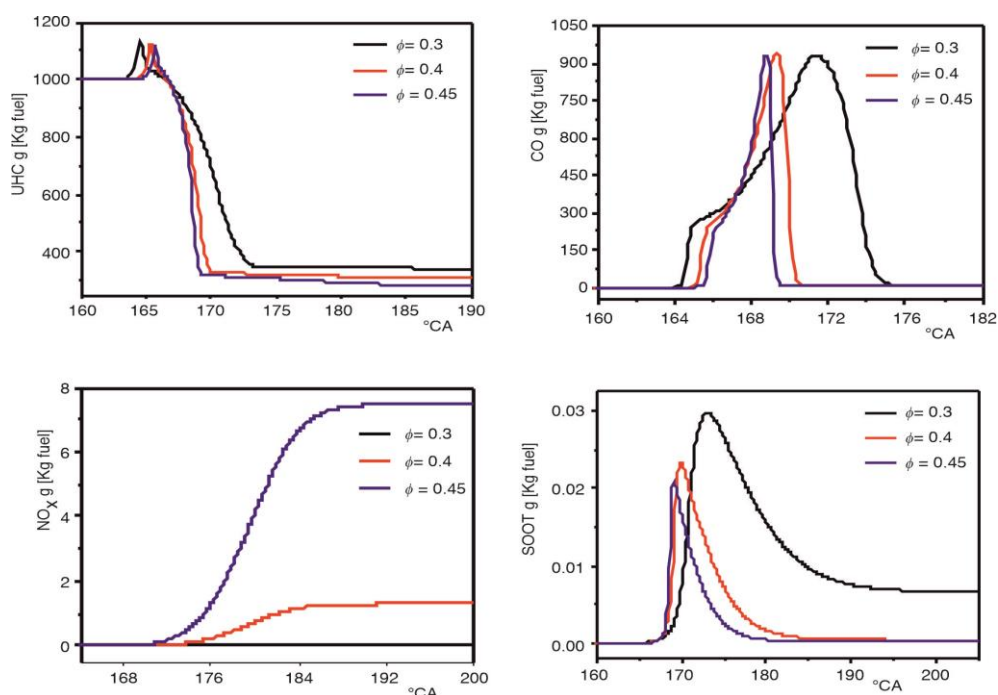


Figure 9. The results of fuel equivalence ratio change

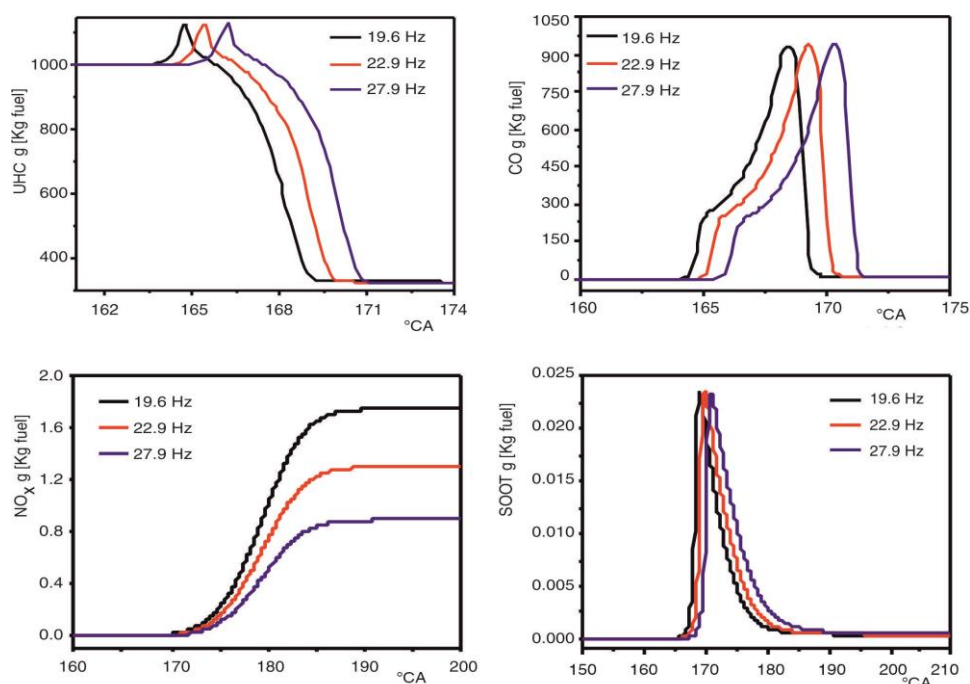


Figure 10. The results of working frequency change

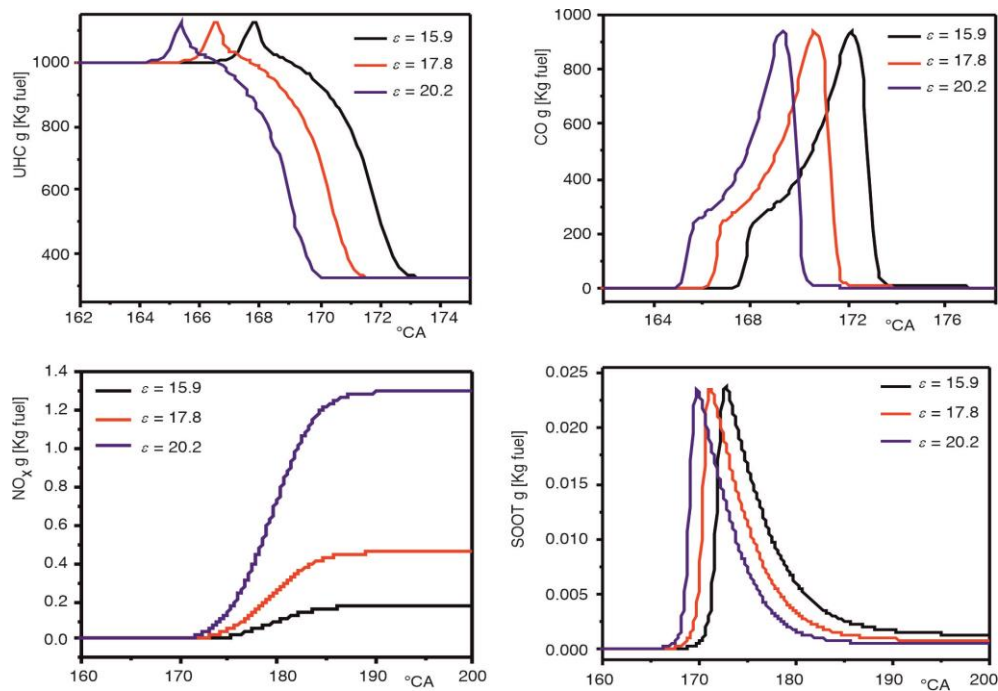


Figure 11. The results of compression ratio change

## Conclusions

The simulation results obtained were summarized as follows.

- These five parameters have a significant impact on HCCI combustion performance of FPEG, and these values determine whether it is a complete two-stage auto-ignition.
- The changes of parameters cause the change of the FPEG combustion phase, further lead to different heat release rate, in-cylinder pressure and temperature.
- The emission is closely related to the combustion process, and the production of NO<sub>x</sub> is sensitive to all parameters, while the production of SOOT is sensitive to only fuel equivalence ratio.

## Acknowledgment

This work was supported by the Talent introduction Project of Anhui Science and Technology University (RCYJ201902), the Key Excellent Young Teachers Program of Universities of Anhui Province (gxyqZD2019059) and the College Students' Innovative Entrepreneurial Training Plan Program (S202010879274 and S202010879290).

## Reference

- [1] Yao, M. F., et al., Progress and Recent Trends in Homogeneous Charge Compression Ignition (HCCI) Engines, *Prog Energ Combust*, 35 (2009), 5, pp. 398-437
- [2] Maurya, R. K., et al., Statistical Analysis of the Cyclic Variations of Heat Release Parameters in HCCI Combustion of Methanol and Gasoline, *Appl Energ*, 89 (2012), 1, pp. 228-236
- [3] Komninos, N. P., et al., Improvement and Validation of a Multi-Zone Model for HCCI Engine Combustion Concerning Performance and Emissions, *Energ Convers Manage*, 49 (2008), 10, pp. 2530-2537
- [4] Ebrahimi, R., et al., An Experimental Investigation on Engine Speed and Cyclic Dispersion in an HCCI Engine, *Fuel*, 89 (2010), 8, pp. 2149-2156

- [5] Tanaka, S., *et al.*, Two-Stage Ignition in HCCI Combustion and HCCI Control by Fuels and Additives, *Combust Flame*, 132 (2003), 1, pp. 219-239
- [6] Mikalsen, R., *et al.*, The Design and Simulation of a Two-Stroke Free-Piston Compression Ignition Engine for Electrical Power Generation, *Appl Therm Eng*, 28 (2008), 5, pp. 589-600
- [7] Zhao, Z., *et al.*, An Experimental Study of the Hydraulic Free Piston Engine, *Appl Energy*, 99 (2012), Nov., pp. 226-33
- [8] Mikalsen, R., *et al.*, A Review of Free-Piston Engine History and Applications, *Appl Therm Eng*, 27 (2007), 14, pp. 2339-2352
- [9] Hanipah, M. R., *et al.*, Recent Commercial Free-Piston Engine Developments for Automotive Applications, *Appl Therm Eng*, 75 (2015), Jan., pp. 493-503
- [10] Jia, B., *et al.*, Design and Simulation of a Two- or Four-Stroke Free-Piston Engine Generator for Range Extender Applications, *Energy Convers Manage*, 111 (2016), Dec., pp. 289-298
- [11] Tsolakis, A., *et al.*, Engine Performance and Emissions of a Diesel Engine Operating on Diesel-RME (Rapeseed Methyl Ester) Blends with EGR (Exhaust Gas Recirculation), *Energy*, 32 (2007), 11, pp. 2072-2080
- [12] McCormick, R. L., *et al.*, Effect of Several Oxygenates on Regulated Emissions from Heavy-Duty Diesel Engines, *Environ. Sci. Technol*, 21 (1997), 4, pp. 1144-1150
- [13] Westbrook, C. K., *et al.*, Chemical Kinetic Modeling Study of the Effects of Oxygenated Hydrocarbons on Soot Emissions from Diesel Engines, *J. Phys. Chem. A*, 110 (2006), 21, pp. 6912-6922
- [14] Zhang, S. L., *et al.*, Stability Analysis of Hydraulic Free Piston Engine, *Appl Energy*, 157 (2015), C, pp. 805-813
- [15] Xu, Z. P., *et al.*, Prototype Testing and Analysis of a Novel Internal Combustion Linear Generator Integrated Power System, *Appl Energy*, 87 (2010), 4, pp. 1342-1348
- [16] Jia, B. R., *et al.*, An Experimental Investigation into the Starting Process of Free-Piston Engine Generator, *Appl Energy*, 157 (2015), Mar., pp. 798-804
- [17] Feng, H., *et al.*, Research on Combustion Process of a Free Piston Diesel Linear Generator, *Appl Energy*, 161 (2016), Jan., pp. 395-403
- [18] Luo, Z., *et al.*, A Reduced Mechanism for Biodiesel Surrogates for Compression Ignition Engine Applications, *Fuel*, 99 (2012), Sept., pp. 143-153